energies

Article

Numerical Investigation into the Effects of Design Parameters on the Flow Characteristics in a Turbine Exhaust Diffuser

Byung Ju Lee [1] and Jin Taek Chung [2,*]

[1] Department of Mechanical Engineering, Graduate School of Korea University, Seoul 02841, Korea; jdbjlee11@korea.ac.kr
[2] Department of Mechanical Engineering, Korea University, Seoul 02841, Korea
* Correspondence: jchung@korea.ac.kr; Tel.: +82-2-921-3364

Abstract: In this study, we numerically investigated the effects of design parameters, such as the strut geometry or diffusion angle, on the performance of an industrial turbine exhaust diffuser. Turbine exhaust diffusers are commonly used to change the kinetic energy of exhaust gases from the outlet of turbine stages into the static pressure. The turbine exhaust diffuser investigated in this work consisted of an annular diffuser with five identical struts equally spaced around the front circumference and a conical diffuser with a hub extension at the rear. Four design parameters were considered and several values for each parameter were tested in this study. The aerodynamic performances of the studied diffusers were evaluated according to their pressure recovery coefficients and rates of total pressure loss. Contours for the velocity, pressure, and entropy increase were plotted and compared for the various diffuser shapes. The numerical results showed that the strut thickness and the axially swept angle of the strut significantly influence the aerodynamic performance of the turbine exhaust diffuser, whereas the strut lean angle and the diffuser hade angle are less important.

Keywords: turbine exhaust diffuser; strut geometry; diffuser hade angle; aerodynamic performance; pressure recovery

Citation: Lee, B.J.; Chung, J.T. Numerical Investigation into the Effects of Design Parameters on the Flow Characteristics in a Turbine Exhaust Diffuser. *Energies* **2021**, *14*, 5171. https://doi.org/10.3390/en14165171

Academic Editor: Andrea De Pascale

Received: 6 July 2021
Accepted: 18 August 2021
Published: 21 August 2021

1. Introduction and Literature Review

The purpose of exhaust diffusers on industrial gas turbines is to convert the kinetic energy of exhaust gas exiting the turbine outlet into static pressure. Since the conditions at the outlet are usually just the atmospheric conditions, pressure recovery causes a reduction in turbine outlet pressure, which increases the efficiency and output of the gas turbine. Exhaust diffusers in large-scale gas turbines are generally axial or annular types, while those used in small gas turbines or gas turbines for offshore plants tend to be radial or quadrilateral types. One of the important features of gas turbine diffusers is the presence of a structure called a strut in the flow path. Struts are necessary for structural reasons, such as for supporting the rotor bearings of gas turbines or for installing pipe systems.

Previously, a wide range of studies have been conducted to improve the performance of turbine diffusers, that is, to convert the kinetic energy of the flow at the turbine outlet into pressure energy while minimizing losses. Previous research can be classified into studies that focus on diffuser or strut shape changes and studies that focus on diffuser inlet flow control.

Ubertini et al. [1] experimentally investigated how the presence of struts affects annular diffuser performance. It was shown that using struts reduces the cross-sectional area, allowing the flow to diffuse more. Struts, however, generated greater diffusion losses, resulting in a drop in system efficiency. Vassiliev et al. [2] tested the effect of two-stage struts on gas turbine diffuser performance when an inlet guide vane was installed between the end of the gas turbine and the diffuser strut to change the angle of incidence and the Mach number of flows entering the diffuser inlet. It was found that while the pressure recovery at the diffuser was basically independent of the inlet Mach number, it was affected by the inlet swirl flow. Based on these results, Vassiliev et al. [3] sought to design a diffuser strut suitable for improved gas turbine operating conditions. The operating conditions were changed by upgrading the existing gas turbine. The existing diffuser suffered from high total pressure loss under the new operating conditions. To tackle this problem, the struts were redesigned using optimization techniques to make them more suitable for the flow characteristics of the new operating conditions.

Sieker et al. [4] investigated the effects of turbine blade wake on flow separation and pressure recovery. Kluß et al. [5] confirmed the effects of interactions between the wake and secondary flow on turbine diffuser performance through an unsteady numerical simulation. Pradeep et al. [6] attempted to improve the performance of the diffuser by changing the strut profile and changing the diffuser shroud face design.

Babu et al. [7] evaluated the improvement in the aerodynamic performance of a turbine exhaust diffuser after adding an elliptical hub extension to the rear of the hub. Hirschmann et al. [8] attempted to improve the performance by combining two different types of diffusers with two cylindrical hub extensions of different lengths. They conducted a computational analysis for all four cases to verify the effects. Schaefer et al. [9] derived the optimal strut shape for existing gas turbine diffusers and the optimal shroud shape for the duct through a multi-purpose optimization method. They compared their results with existing models through computer analysis.

Vassiliev et al. [10] confirmed that inlet flow conditions, such as the Mach number, total pressure distribution, flow angle, and turbulence intensity have a great influence on the internal flow through the diffuser by using computational analysis, league tests, and measurements taken from a real-world engine. Hirschmann et al. [11] confirmed the effect of the total pressure distribution at the inlet of the diffuser on gas turbine diffuser performance through both experimental and computational analysis. The velocity distribution at the diffuser's longitudinal section was confirmed by creating a setup with a uniform total pressure distribution at the diffuser inlet, a setup with a total pressure distribution that was stronger at the hub, and a setup with a total pressure distribution that was stronger at the tip. Dobhal et al. [12] investigated the improvement in turbine diffuser performance that comes from modifying the diffuser shape in terms of the strut back angle, hub surface extension, and reduction in duct length.

Xu et al. [13] investigated the influence of the inlet flow conditions on the exhaust diffusers of steam turbines using computational fluid dynamics (CFD). The two exhaust diffusers investigated in their study had different area ratios and axial lengths. The numerical results showed that inlet flow produced sufficiently high velocity jets due to tip leakage flow from the last stage rotor, which was found to play a role in avoiding flow separation near the diffuser casing. Schaefer et al. [14] investigated the effects of inhomogeneous inlet flow on gas turbine diffusers through experiments and computational analysis. Three inlet flows with different inlet blockage factors were set up to analyze the flow field inside the diffuser and their effect on the pressure recovery coefficient. Vassiliev et al. [15] investigated the flow characteristics of a turbine exhaust diffuser with two-stage struts and modifications at the off-design conditions. Radial splitters were installed at the first-row struts or at the second-row struts while the central body was removed. Neither modification was found to be effective in reducing the loss at the design point, but a slight reduction in pressure loss was achieved with the radial splitter modification at the strong off-design point relative to the original design.

Rasouli et al. [16] conducted experiments and computational analysis on four types of hub extension: cone, ellipsoid, hollow cylinder, and cylinder extensions. The diffuser with the hollow cylinder hub extension achieved the best performance. Xue et al. [17] investigated turbine exhaust diffuser/collectors with three different types of diffuser strut: no strut, profiled strut, and cylindrical strut; these were tested while changing the inlet swirl angle. The experiments showed that the diffuser/collector system with the profile strut was best over a broad range of inlet swirl angles. Siorek et al. [18] numerically studied the performance of gas turbine exhaust diffuser-collectors at off-design conditions. The strut stagger angle as well as the inlet swirl angle were changed to evaluate their effect on diffuser performance. Mihailowitsch et al. [19] numerically investigated interactions between the last stage of a turbine with a shrouded rotor and the subsequent diffuser at part-load, design-load, and over-load conditions. Three different seal gap widths were also considered to control leakage flow. The results showed that the optimum gap width was operating point-dependent in terms of the efficiency of the whole system, but the turbine's best performance occurred when the rotor had the minimum gap width. Three operating conditions: part-load, design-load, and over-load, were also investigated experimentally and numerically by Bauer et al. [20].

The previous studies discussed above tend to focus on the inflow conditions, especially the wake or swirl angle of the working fluid; however, few studies have investigated the effects of strut geometry. Strut geometry should be considered in view of the aerodynamics because struts interfere with the flow of the combustion gas in the diffuser, and the pressure recovery of the gas can decrease. The amount of pressure recovery is determined by not only the diffusion angle, but also the strut geometry. The research objectives of this study were to find the correlation between the strut and diffuser geometry and the pressure recovery and pressure loss of combustion gas by using computational fluid dynamics (CFD). Four design parameters related to the strut design or diffusion angle of the turbine exhaust diffuser for a H-class gas turbine were considered. The turbine exhaust diffusers we investigated included an annular diffuser with five simple struts, a manifold section with a hub extension, and a conical diffuser. The predicted design condition at the last-stage rotor outlet as well as ideal gas mixtures, including carbon dioxide and steam were considered in our real-scale computations, while off-design conditions were not considered in this study.

The turbine exhaust diffuser geometry and four design parameters are introduced in Section 2. Section 3 describes the numerical methodology including the computational domain, mesh generation, boundary conditions, and numerical validation. The influence of each design parameter on the aerodynamic performance is investigated in Section 4. Section 5 concludes the present study.

2. Geometry of Turbine Exhaust Diffuser

The reference turbine exhaust diffuser we considered is designed for H-class gas turbines with a generating capacity of 200 MW. The exhaust diffuser was designed to avoid structural problems while trying to achieve the best aerothermal properties. Also, it was designed as simply as possible to make it easy to install various facilities and pipes for driving the gas turbine.

The reference turbine exhaust diffuser is an annular diffuser with five struts upstream, a cylindrical manifold section with a hub extension in the middle and a conical diffuser, as shown in Figure 1. The struts are arranged at 72° intervals, their leading edges have an elliptical shape while the trailing edge is rectangular. The struts have a lean angle of 0°, an attack angle of 0°, and an axially swept angle of 80°. In the annular diffuser domain, diffusion due to increasing cross-sectional area occurs twice; the primary diffusion angle was set to 19° while the secondary diffusion angle was set to 12°. The hub extension in the manifold section has a hollow cylinder shape in which the hub of the annular diffuser domain is extended. The diffusion angle of the conical diffuser was fixed at 5° and the total axial length was also fixed.

Several strut design parameters (thickness, lean angle, axially swept angle) and the diffusion angle of the annular diffuser play an important role in determining the performance of the turbine exhaust diffuser. As such, the aforementioned four design parameters, which are shown in Figure 2, were chosen to investigate how the aerodynamic performance changed according to each of the design factors using CFD. The design target in this study was to achieve a pressure recovery coefficient of 0.75 or more with a rate of total pressure loss of 4% or less.

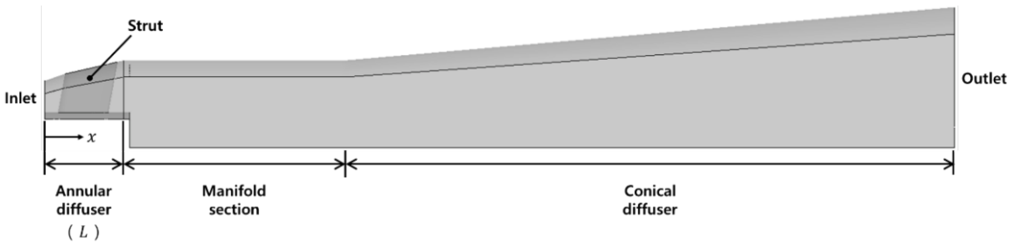

Figure 1. The schematic of the reference turbine exhaust diffuser.

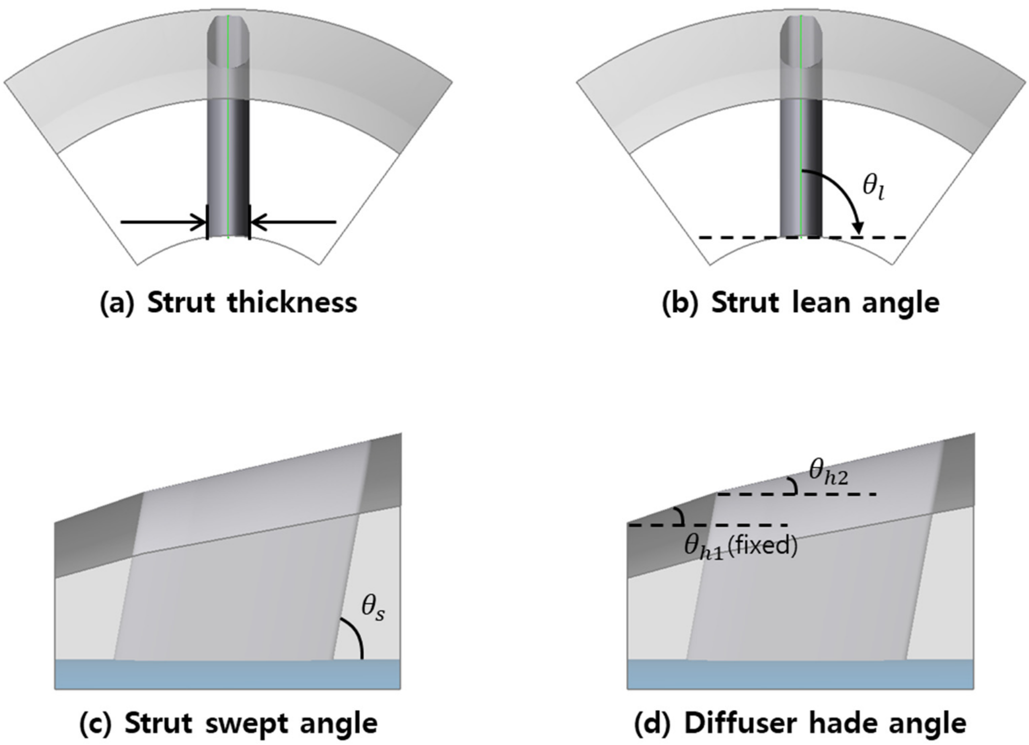

Figure 2. Four design parameters that were varied in the industrial turbine exhaust diffuser.

3. Computational Method

3.1. Computational Domain and Mesh Generation

To reduce the computational time, only one-fifth of the circular passage containing one strut was considered as the computational domain to reduce the total number of points in the mesh. The hexahedral mesh of the annular diffuser domain, as shown in Figure 3, was created using commercial software called ANSYS Turbogrid V16.2. The hexahedral mesh of the manifold section and the conical diffuser domain, as shown in Figure 4, was generated by ANSYS ICEM-CFD V16.2. The two domains have 1.46 million and 3.32 million grid points, respectively, and the number of points in each mesh was determined by grid independency tests, which are discussed in Section 3.4. In order to improve calculation accuracy for boundary layer flow, the meshes were denser near the wall so that y+, the dimensionless distance from the wall to the first node, was 2 or less in all regions.

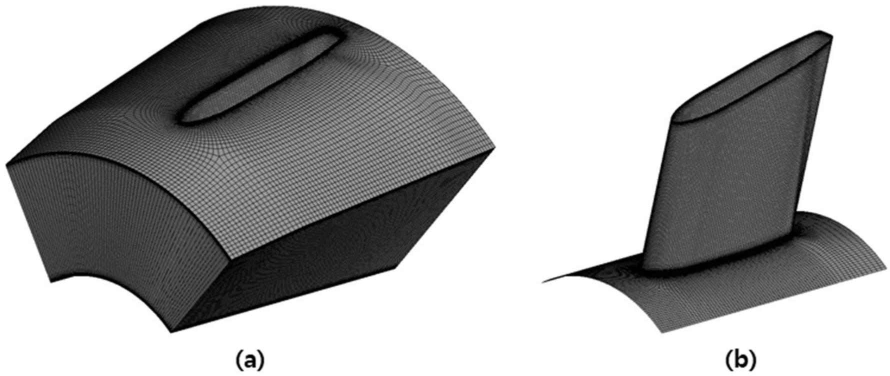

Figure 3. Mesh structure for the annular diffuser domain: (**a**) external, (**b**) hub and strut.

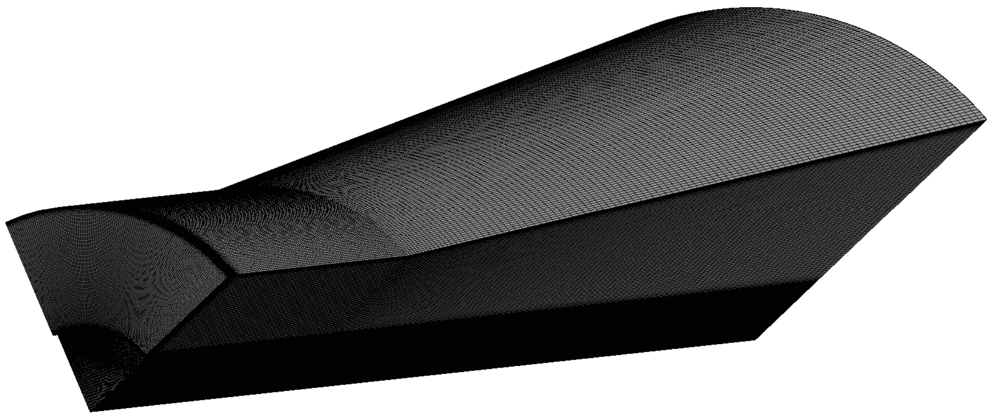

Figure 4. Mesh structure for the manifold section and conical diffuser domain.

3.2. Boundary Conditions

To predict the aerodynamic performance of the turbine exhaust diffuser, the 3D steady Reynolds-averaged Navier–Stokes equations were solved using ANSYS CFX V16.2. The total pressure, total temperature, flow angle, turbulent kinetic energy, and turbulent eddy frequency distribution according to the span predicted downstream of the last turbine stage were given as the inlet boundary conditions. Figure 5 shows the graph of the inlet boundary conditions. The design mass flow rate of the industrial gas turbine was used as the outlet boundary condition. The boundaries, that is, the wall surfaces of structures like the strut, hub and shroud, were assumed to have no slip, smooth walls and to be adiabatic. The working fluid was set to an ideal gas mixture including argon, carbon dioxide, steam, oxygen, and nitrogen; each gas in the mixture satisfied the ideal gas equation. The specific heat capacity and dynamic viscosity of each gas were set to the NASA format and Sutherland's formula [21], respectively. The mass fractions of each gas component predicted downstream of the last turbine stage are listed in Table 1. The $k-\omega$ SST (shear stress transport) turbulence model, which is widely used for turbomachinery applications [22–26], was used as the turbulence model. The domain interface used between the outlet of the annular diffuser and the inlet of the manifold section followed the frozen rotor method because the shape of the two interface surfaces were not exactly the same. If the domain interface is set to none in this situation, the ANSYS CFX-Solver will recognize the non-adjacent parts as a wall. The convergence of the steady-state simulations was set to 1×10^{-4} for the root mean square residuals of all the governing equations. The mass, momentum, energy and turbulence equations were treated with a high-resolution advection scheme.

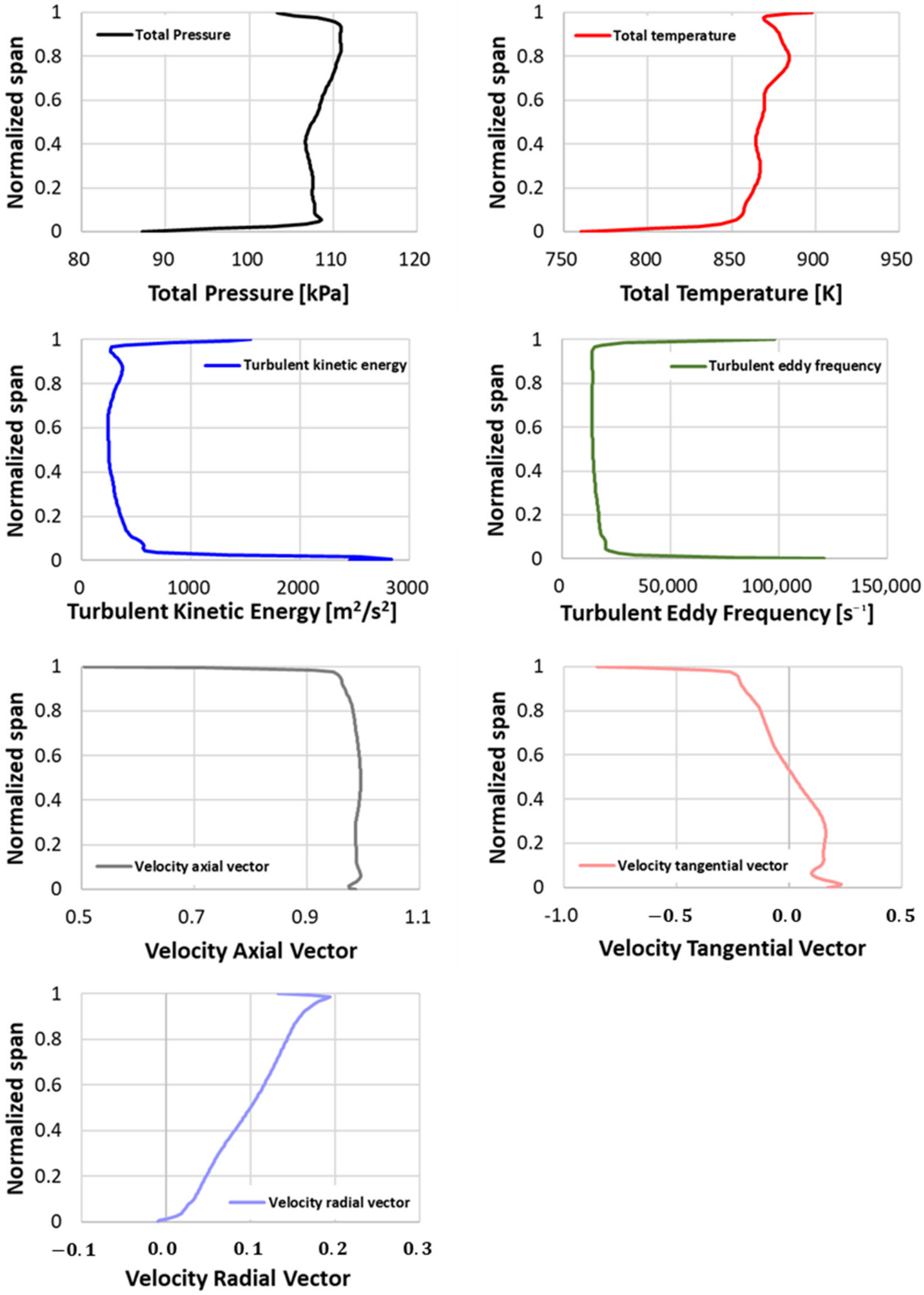

Figure 5. Inlet boundary conditions.

Table 1. Mass fractions of each gas component in the combustion gas mixture.

Gas Component	Argon	CO_2	H_2O	O_2	N_2
Mass fraction	0.01249	0.06364	0.05658	0.13251	0.73478

3.3. Performance Evaluation

The pressure recovery coefficient (C_p) and the rate of total pressure loss ($C_{pt,loss}$) were used to evaluate the performance of the turbine diffuser, the definition of each is as follows.

$$C_p = \frac{p_{s,out} - p_{s,in}}{p_{t,in} - p_{s,in}} \tag{1}$$

$$C_{pt,loss} = \frac{p_{t,in} - p_{t,out}}{p_{t,in}} \times 100\ [\%] \tag{2}$$

In the equations, $p_{t,in}$ and $p_{t,out}$ are the mass flow averaged total pressure at the inlet and outlet, respectively, while $p_{s,in}$ and $p_{s,out}$ are the mass flow averaged static pressure at the inlet and outlet, respectively. For a detailed analysis of the internal flow field through the turbine exhaust diffuser, several cross-sectional planes were used to show the distribution of the C_p and $C_{pt,loss}$ or calculate the mass-averaged C_p and $C_{pt,loss}$. The axial distance of the cross-sectional planes, expressed by x, was normalized according to the length of the annular diffuser, L. In addition, two internal longitudinal sections were also used to evaluate the velocity distribution. Plane 1 was designated to pass through the center of the strut, while plane 2 was designated between two of the struts. The angle between the two planes was set to 30°.

3.4. Grid Independency and Turbulence Model Test

The number of points in the mesh of the annular diffuser domain with the reference strut as well as the manifold section and conical diffuser domain were determined by the grid independency tests, the results of which are shown in Table 2. The $k - \omega$ SST turbulence model was used for these tests. The mass-averaged static pressure at the outlet were compared for different size meshes, and its value was found to increase as the number of points in the mesh increased. The relative error of the result for the very fine mesh to the result for the fine mesh was insignificant. Therefore, a fine mesh was chosen for the computational grids in this study as it had the best balance between accuracy and computational cost.

Table 2. Grid independency tests.

	Total Number of Mesh	**Mass-Averaged Static Pressure [Pa]**	**Relative Error [%]**
Very coarse	612,828	103,140	−0.164
Coarse	1,587,128	103,199	−0.106
Moderate	2,699,986	103,250	−0.057
Fine	4,774,610	103,294	−0.015
Very fine	6,063,871	103,309	-

The turbulence model test with the fine mesh selected from the grid independency tests was conducted using standard $k - \epsilon$, standard $k - \omega$, and $k - \omega$ SST models to determine the turbulence closure. In order to compare the experimental results with the numerical results, the mass-averaged C_p was plotted over the normalized distance of the cross-sectional planes, as shown in Figure 6. When the standard $k - \epsilon$ turbulence model was applied, the mass-averaged C_p was overpredicted compared to the experiment for the whole section. The standard $k - \omega$ turbulence model, on the other hand, generally underestimated the mass-averaged C_p. The $k - \omega$ SST was found to be the most accurate turbulence model so this was applied in the simulations in this study.

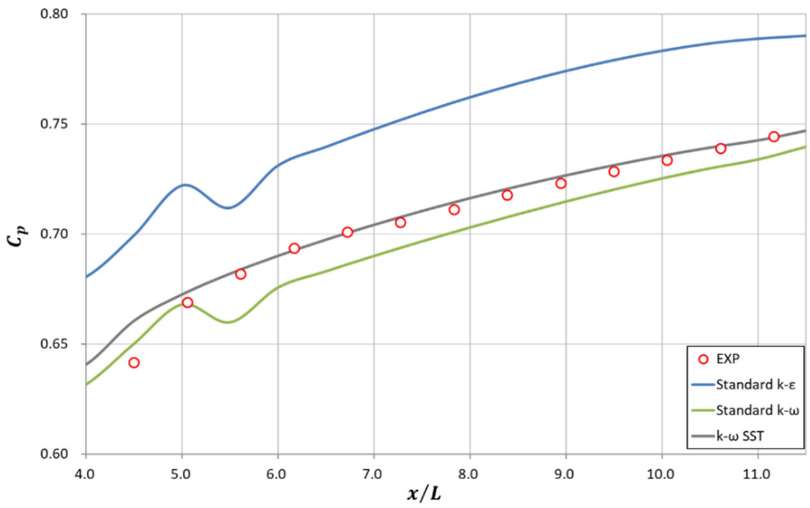

Figure 6. C_p plot for the turbulence model test.

4. Parametric Study

4.1. Strut Thickness

Figure 7 shows the shape of the reference strut and the five derived struts. The shape chosen for the strut leading edge was half an ellipse. The major axis of the elliptical leading edge of the reference strut is over three times longer than the minor axis, and the strut thickness is maintained when we move behind the minor axis of the half ellipse. The trailing edge thickness of the strut in the reference strut gradually decreases in a taper as we move backwards, but the trailing edges of the five derived struts have no taper and are rectangular. The strut thickness of the Case_T1 strut is the same as the reference strut, while each of the other derived struts shows a consecutive increase of 13% over the previous case. Other design parameters, such as the major axis of the strut leading edge are the same as the reference strut. Details of the strut geometries are shown in Table 3.

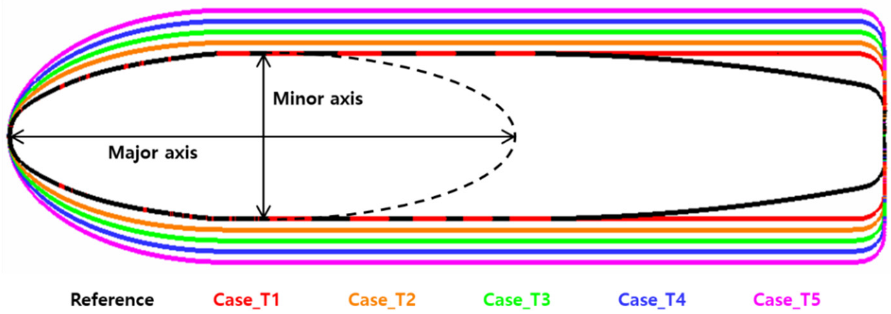

Figure 7. Schematic of the reference and derived struts with varying thicknesses.

Table 3. Geometric information for the reference and derived struts with varying thicknesses.

Strut	Major Axis Length of Strut LE	Minor Axis Length of Strut LE	Strut Thickness
Reference	3.183	1	$1 \rightarrow 0.5$
Case_T1	3.183	1	1
Case_T2	3.183	1.1305	1.1305
Case_T3	3.183	1.2610	1.2610
Case_T4	3.183	1.3915	1.3915
Case_T5	3.183	1.5220	1.5220

The mass-averaged C_p and $C_{pt,loss}$ plots when using struts with varying thicknesses over the normalized distance of the cross-sectional planes are illustrated in Figures 8 and 9, respectively. The plots in Figure 8 indicate that approximately 70% of the pressure recovery was achieved in the annular diffuser. For the reference, Case_T1 and Case_T2 struts, the value of C_p at the conical diffuser outlet was found to be lower than the design target of 0.75; in contrast, the Case_T3 and Case_T4 struts satisfied the design target, with a C_p increase of 3.5% compared to the reference. In addition, it can be seen from Figure 9 that approximately 30% of the total pressure loss was generated in the annular diffuser. All struts met the design target of 4% for $C_{pt,loss}$, while $C_{pt,loss}$ at the conical diffuser outlet increased as the strut thickness increased from the reference to Case_T2, but Case_T3 and Case_T4 did not follow this tendency and showed a decrease in $C_{pt,loss}$. The $C_{pt,loss}$ of Case_T3 measured at the conical diffuser outlet was the lowest, decreasing by 8.9% compared to the reference.

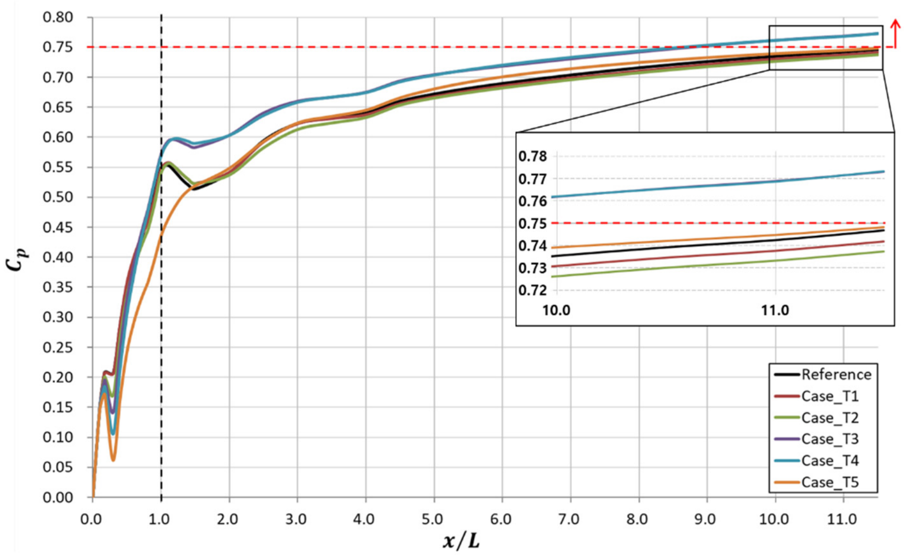

Figure 8. C_p plot for the derived struts with varying thicknesses.

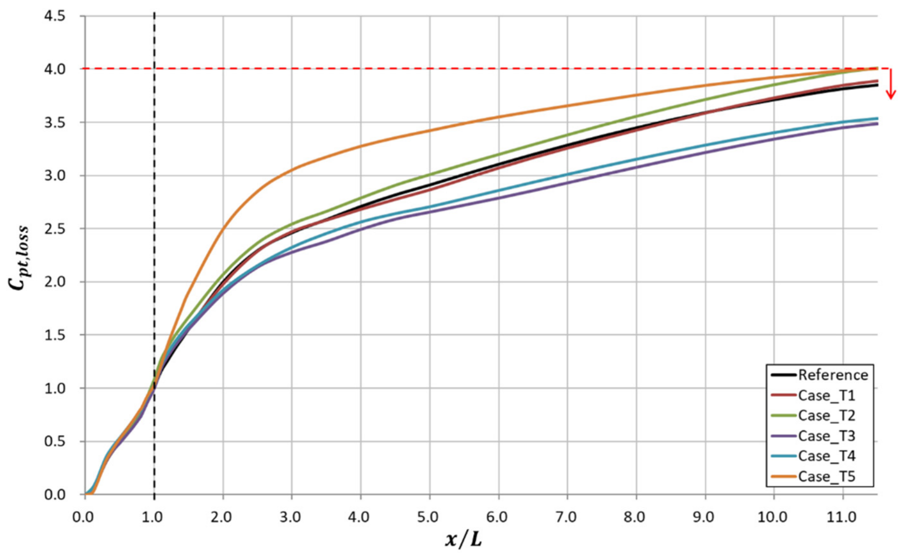

Figure 9. $C_{pt,loss}$ plot for the derived struts with varying thicknesses.

The velocity contours from the two longitudinal sections are shown in Figure 10; these were used to evaluate changes in the flow field at the annular diffuser with changes in strut thickness. It was confirmed that a recirculation zone exists at the center of the manifold section due to rapid expansion. The low-speed region shown in Plane 1 is caused by the wake generated at the strut trailing edge, and becomes wider as the strut thickness increases. This is one of the factors that degrades the performance of the turbine exhaust diffuser. It can be seen that the recirculation zone shown in Plane 2, which originates from the hub at a dimensionless distance of 0.4, gradually decreases as the strut thickness increases. This occurs after a dimensionless distance of 1.0 is reached in the Case_T4 and Case_T5 struts. As the strut thickness increases, the strut passage decreases, resulting in an increase in the velocity of the fluid passing between the struts. This is thought to play a role in delaying the emergence of a recirculation zone downstream, and is one of the factors that increases the performance of the turbine diffuser. Taking into account the two effects that strut thickness has on aerodynamic performance, the Case_T3 strut showed the best performance. This is because the performance enhancement due to the velocity increase between the struts has a greater effect than the performance degradation caused by the decrease in velocity behind the struts.

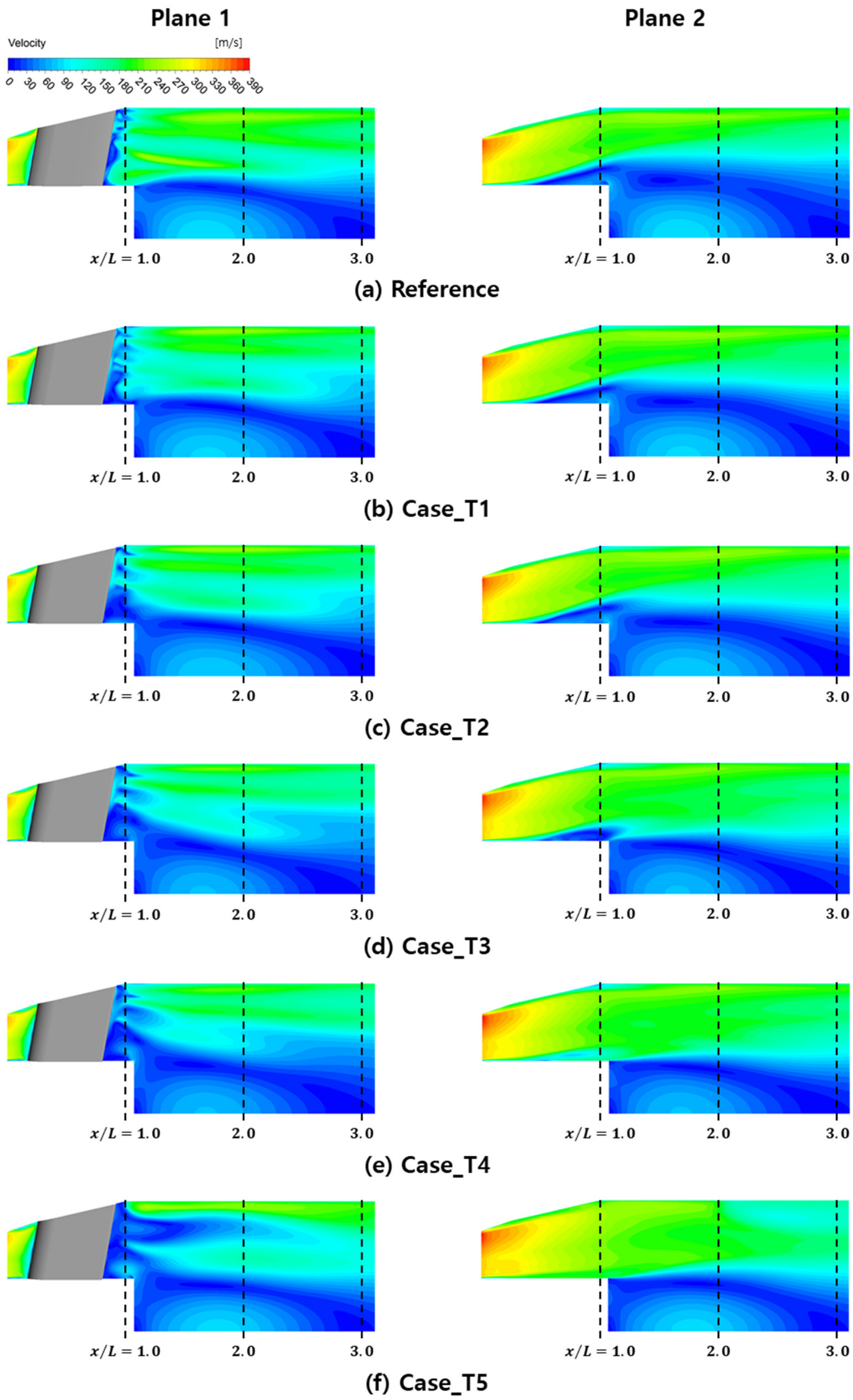

Figure 10. Velocity contours at planes 1 and 2 for the derived struts of varying thicknesses.

The $C_{pt,loss}$ contours at two cross-sectional planes, at normalized distances of 0.4 and 1.0, streamlines and vortex structures inside the annular diffuser are shown in Figure 11. The swirl flow at the inlet of the annular diffuser rotates counterclockwise on the basis of the rotating axis, and it was confirmed that horseshoe vortices are generated by the characteristics of this swirl flow. The horseshoe vortex near the strut hub was found to be on the left side of the strut from the front view, the horseshoe vortex near the shroud is to the right. The total pressure loss identified in region ⓐ shown in Figure 11, appears to be caused by the horseshoe vortex generated near the shroud. The total pressure loss due to flow separation in region ⓑ can be explained in connection to the velocity contours in Plane 2 that are shown in Figure 10. For the Case_T5 strut, in contrast to other struts, the total pressure loss due to backflow was additionally generated in region ⓒ, as shown in Figure 11f. It is thought that the performance degradation due to the velocity decrease behind the struts would be greater than the performance enhancement based on the velocity increase between the struts.

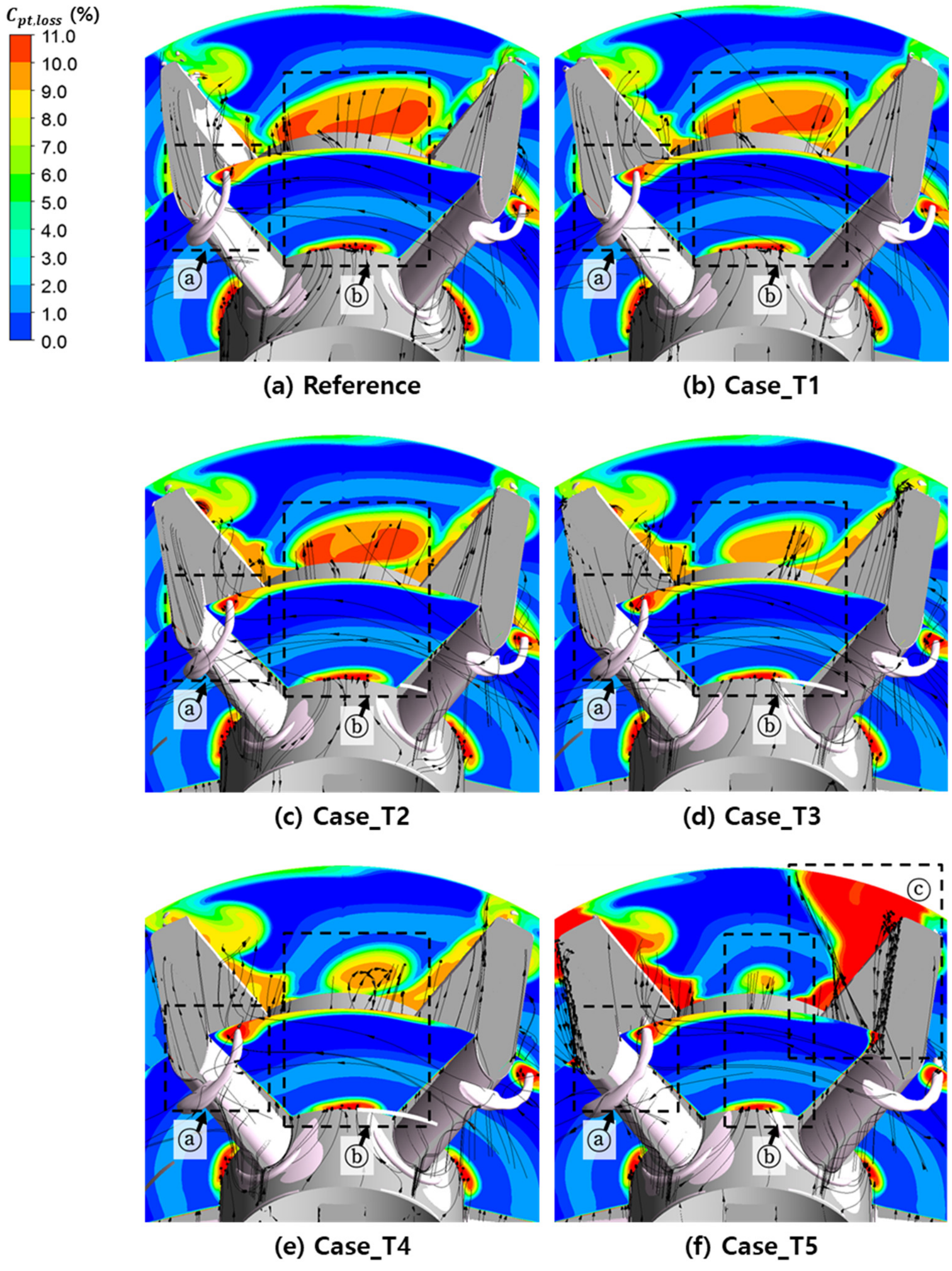

Figure 11. $C_{pt,loss}$ contours at $x/L = 0.4$ & 1.0 for the derived struts of varying thicknesses.

4.2. Strut Lean Angle

The strut lean angle of the reference strut is 0° and the derived struts that lean in the clockwise direction when looking from the inlet are denoted by the lean angle plus (LAP), while the derived struts that lean in the counterclockwise direction are denoted by the lean angle minus (LAM). Lean angles of 15° and 30° were used for both LAP and LAM struts, resulting in a total of four derived struts with varying lean angles. Other design parameters were the same as the reference strut. Illustrations of the four derived struts are shown in Figure 12, while the strut name and the geometric information for each derived strut are shown in Table 4.

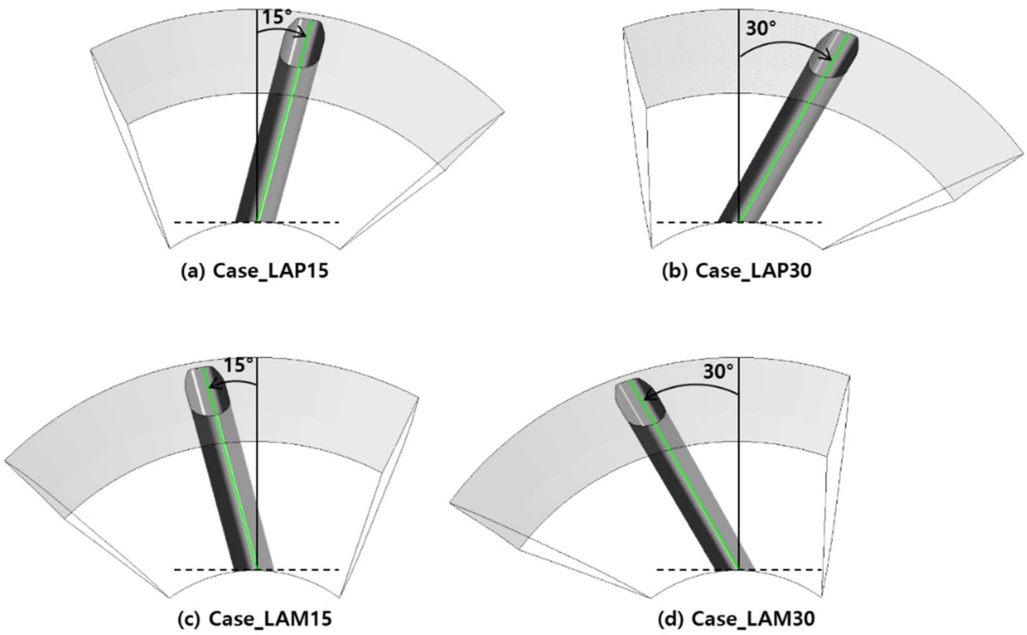

Figure 12. Schematics of the derived struts with varying lean angles.

Table 4. Lean angles of the reference and derived struts.

Strut	Reference	Case_LAP15	Case_LAP30	Case_LAM15	Case_LAM30
Lean angle of strut	0°	+15°	+30°	−15°	−30°

Figures 13 and 14 show the mass-averaged C_p and $C_{pt,loss}$ over the normalized distance of the cross-sectional planes for the struts with various lean angles, respectively. These plots confirm that pressure recovery generally increases as the strut leans in the counterclockwise direction. However, for all the struts, C_p at the conical diffuser outlet was less than the design target of 0.75, including the reference strut. In addition, the $C_{pt,loss}$ at the conical diffuser outlet was found to be less than the design target of 4% for all derived struts except for the LAP30 strut. However, the reference strut had the lowest value for $C_{pt,loss}$ at the conical diffuser outlet, as such it can be concluded that it is difficult to improve aerodynamic performance by changing the strut lean angle.

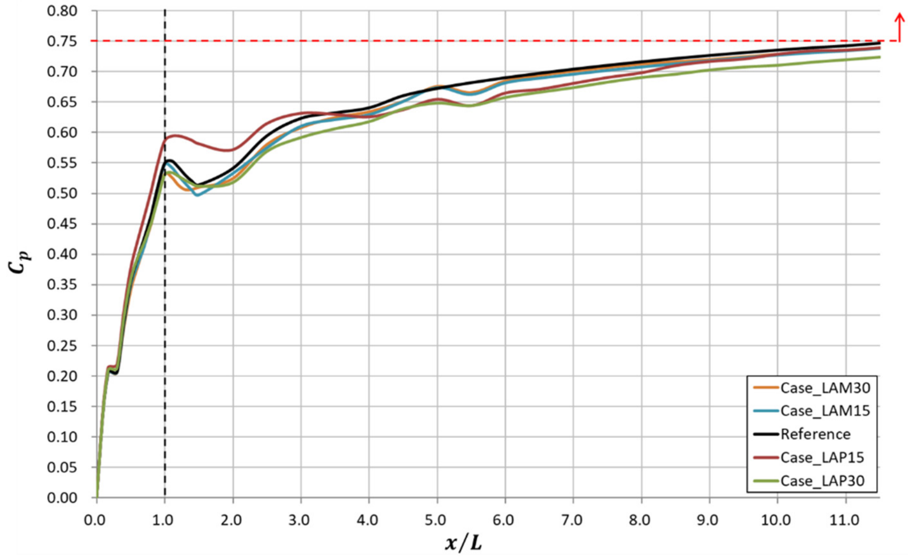

Figure 13. C_p plot for the derived struts with varying lean angles.

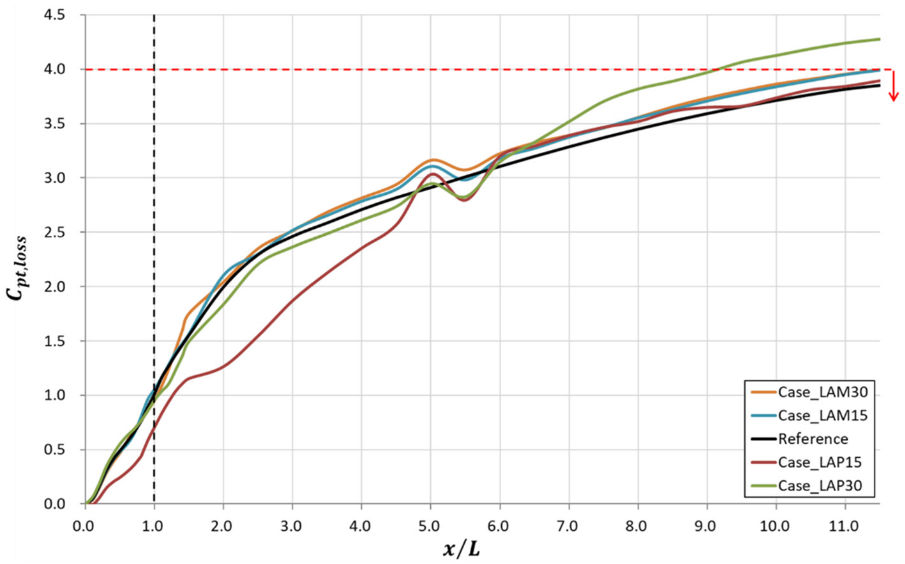

Figure 14. $C_{pt,loss}$ plot for the derived struts with varying lean angles.

In Figure 15, the $C_{pt,loss}$ contours from the point of view of two cross-sectional planes at normalized distances of 0.4 and 1.0, streamlines and vortex structures inside the annular diffuser are shown. The positions of the horseshoe vortex structures near the hub and shroud both are similar to those seen for the derived struts with varying thicknesses. This is because the swirl flow at the annular diffuser inlet is fixed. For the LAM struts, the high total pressure loss region near the hub (ⓐ) due to flow separation is similar to that seen with the reference, and the magnitude of the total pressure loss increases when the counter-clockwise lean angle increases. However, for the LAP struts, the high total pressure loss region is more widely spread. The magnitude of the total pressure loss also increases as the clockwise lean angle increases. Additional high total pressure loss regions ⓑ and ⓒ appear due to the axially reversed flow.

To evaluate the changes in the flow field according to the struts' lean angles, C_p contours at a cross-sectional plane with a normalized distance of 1.0, and $C_{pt,loss}$ contours at a cross-sectional plane with a normalized distance of 5.0 are shown in Figure 16. It can be seen that there is a high C_p region near the shroud while there is a low C_p region near the hub surface, indicating that pressure recovery occurs mostly around the shroud. The low C_p region near the hub of the LAP struts is smaller than for the LAM struts, which is why the C_p difference between the LAP struts and the LAM struts is large. In addition, high $C_{pt,loss}$ occurs at the center for all struts, indicating that the total pressure loss comes mostly from the center due to recirculation flow. The low $C_{pt,loss}$ region near the shroud of the LAP struts is larger than it is for the LAM struts, which is why the $C_{pt,loss}$ difference between the LAP struts and the LAM struts is so large.

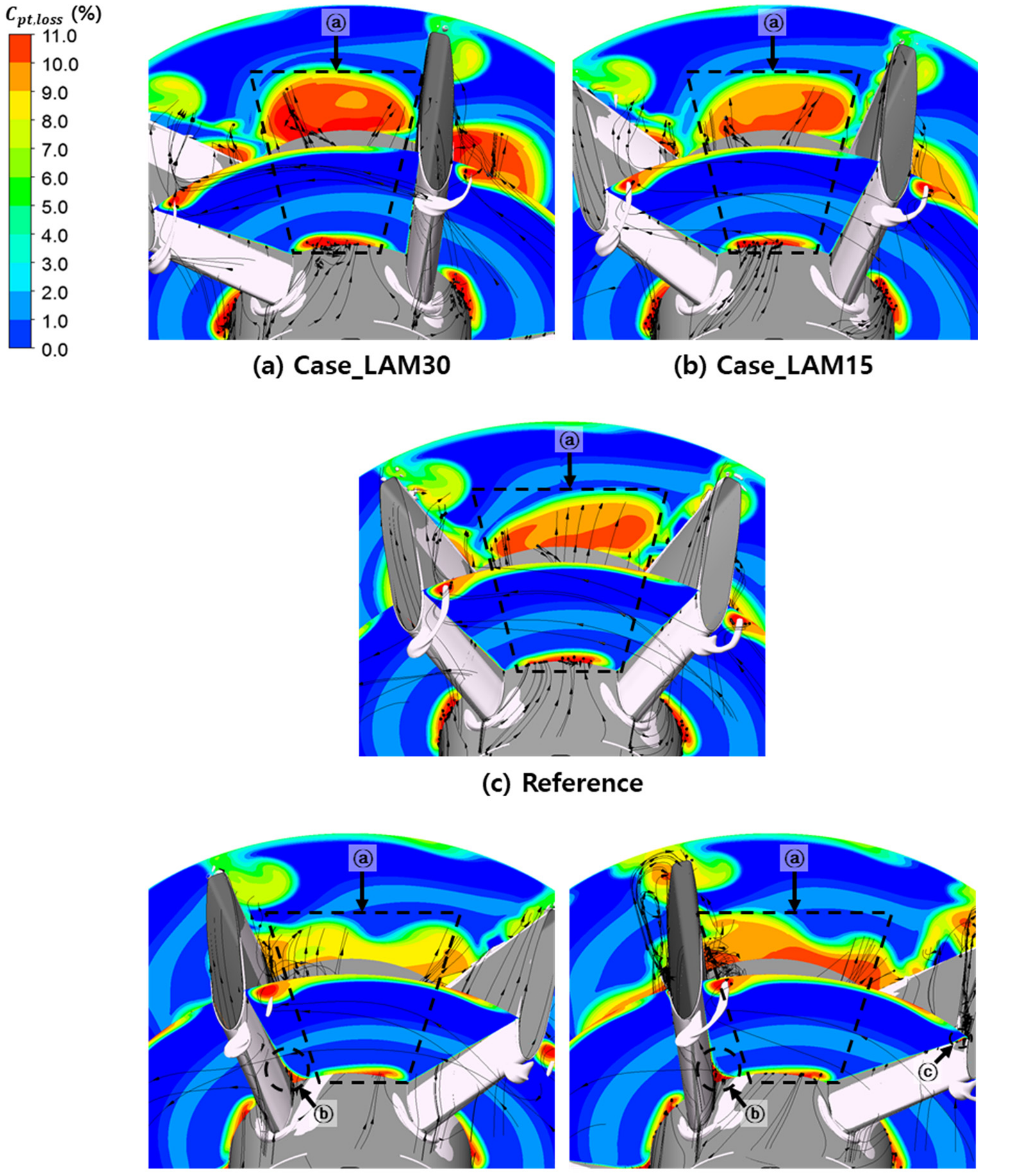

Figure 15. $C_{pt,loss}$ contours at x/L = 0.4 & 1.0 for the derived struts with varying lean angles.

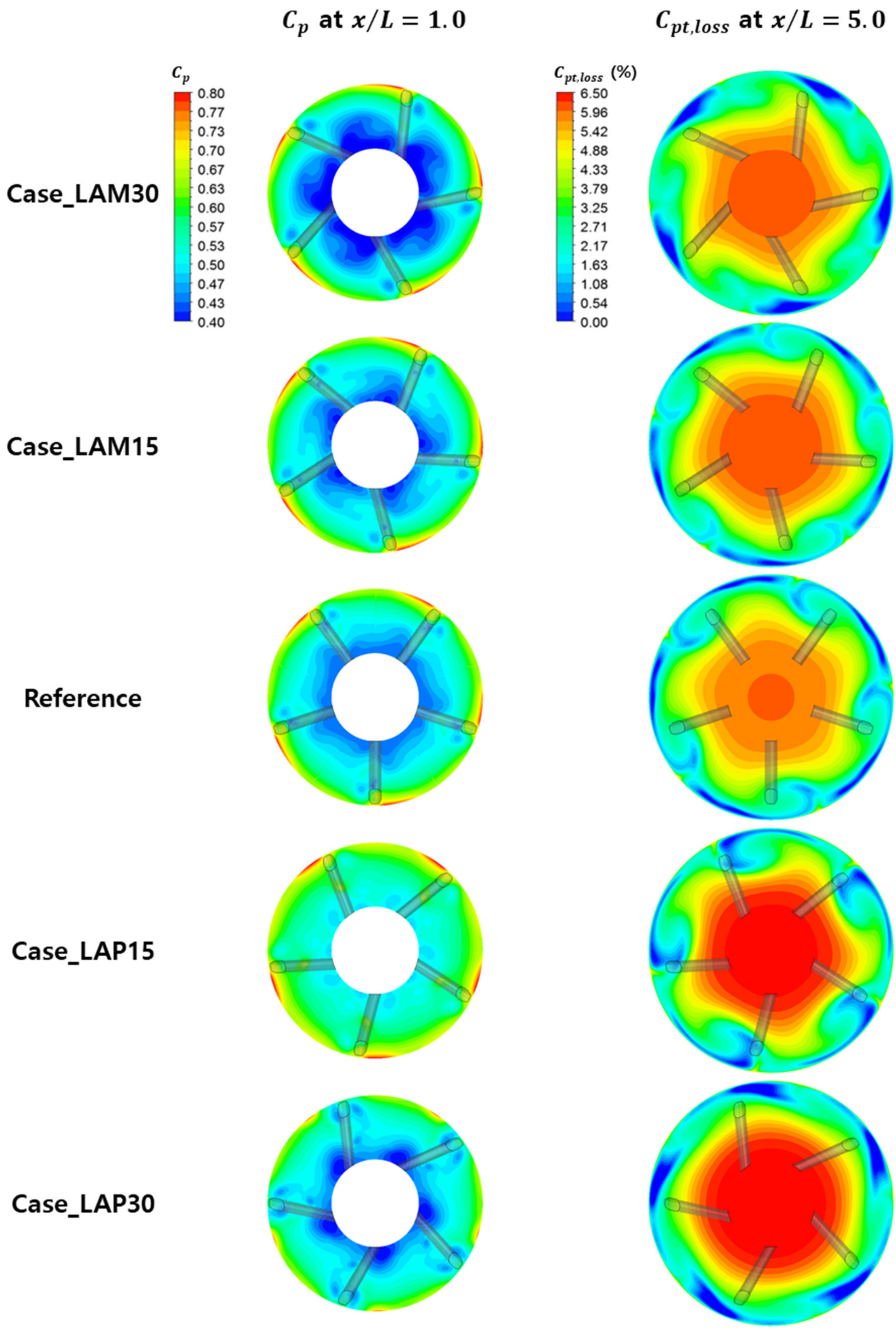

Figure 16. C_p contours at $x/L = 1.0$ and $C_{pt,loss}$ contours at $x/L = 5.0$ for the derived struts with varying lean angles.

4.3. Strut Swept Angle

The angle between the rotation axis and the leading edge, or the trailing edge, of the strut is called the "axially swept angle of the strut" or simply the "strut swept angle". The strut swept angle of the reference strut is 80°. The reference and derived struts with varying strut swept angles are labeled using the prefix ASA (the acronym for axially swept angle) followed by the value of the angle. The shapes of the derived struts are shown in Figure 17, the strut name and shape information for each derived strut are shown in Table 5. Other design parameters are the same as the reference strut.

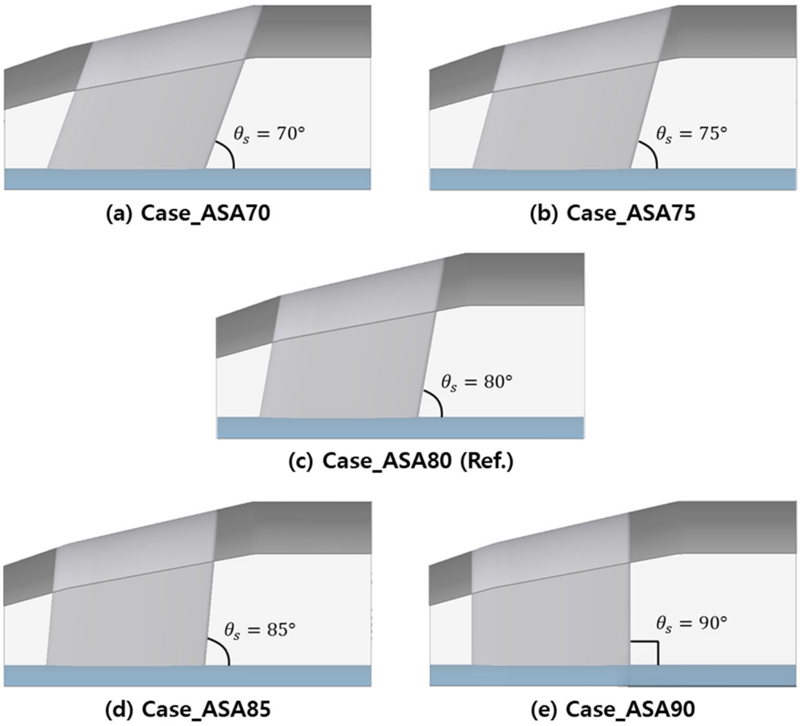

Figure 17. Schematics of the derived struts with varying swept angles.

Table 5. Geometry information for the reference and derived struts with varying swept angles.

Strut	Case_ASA70	Case_ASA75	Case_ASA80 (Ref.)	Case_ASA85	Case_ASA90
Swept angle of strut	70°	75°	80°	85°	90°

The mass-averaged C_p and $C_{pt,loss}$ plots over the normalized distance of the cross-sectional planes for the struts with varying swept angles are illustrated in Figures 18 and 19, respectively. Figure 18 shows that pressure recovery increases as the strut swept angle becomes smaller. ASA70 and ASA75 satisfy the C_p design target of 0.75 or over, while the C_p of the ASA70 strut, which is higher than any other strut, increases by 2.9% compared to the reference strut. In addition, all struts except for ASA90 meet the design target of 4%, while the $C_{pt,loss}$ at the conical diffuser outlet increases as the strut swept angle becomes larger, as shown in Figure 19. The strut with the lowest $C_{pt,loss}$ is ASA70, with a decrease of 7.8% compared to the reference.

The contours viewed from two cross-sectional planes at normalized distances of 0.3 and 0.8, streamlines and vortex structures inside the annular diffuser are shown in Figure 20. The horseshoe vortex structures seen near the hub and shroud are similar to those seen with the derived struts with varying thicknesses and lean angles. The size of the horseshoe vortex decreases as the strut swept angle becomes smaller. The total pressure loss identified in region ⓐ shown in Figure 20 is related to the horseshoe vortex generated near the shroud. Hence, it can be concluded that the high $C_{pt,loss}$ region is reduced as the strut swept angle gets smaller.

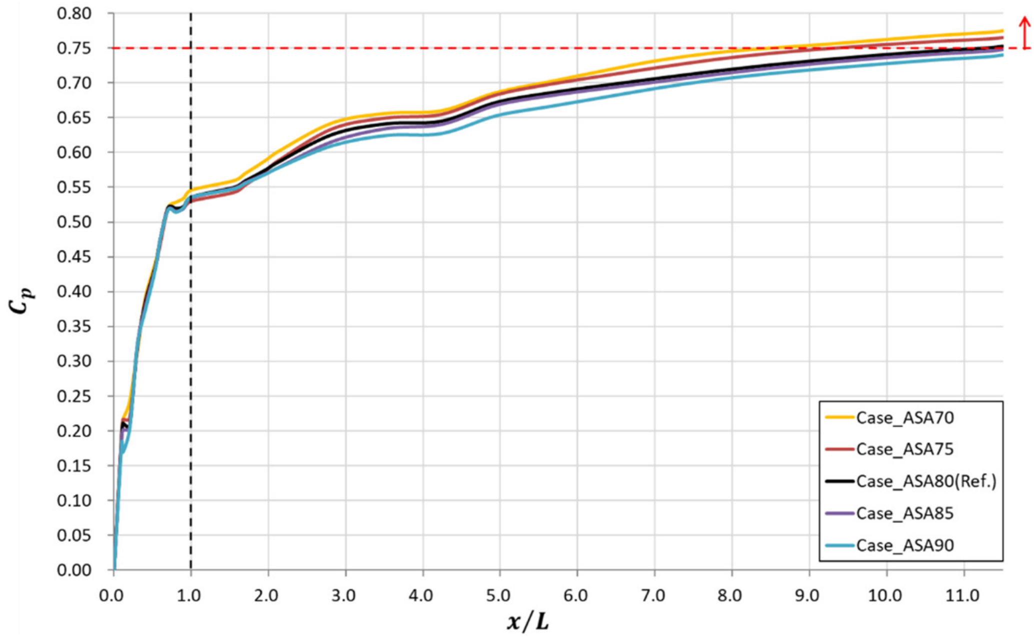

Figure 18. C_p plot for the derived struts with varying swept angles.

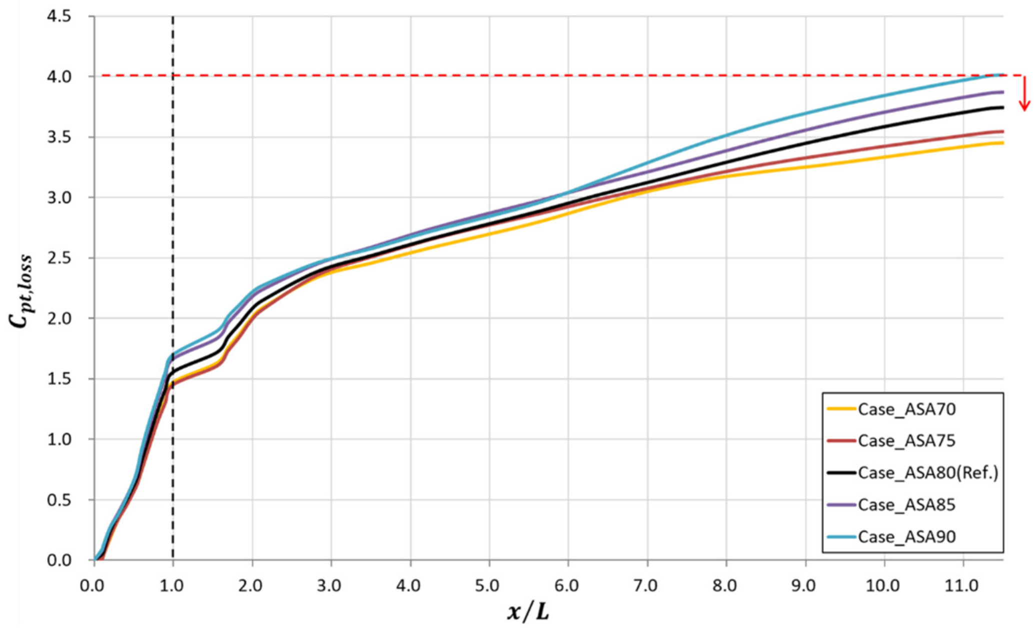

Figure 19. $C_{pt,loss}$ plot for the derived struts with varying swept angles.

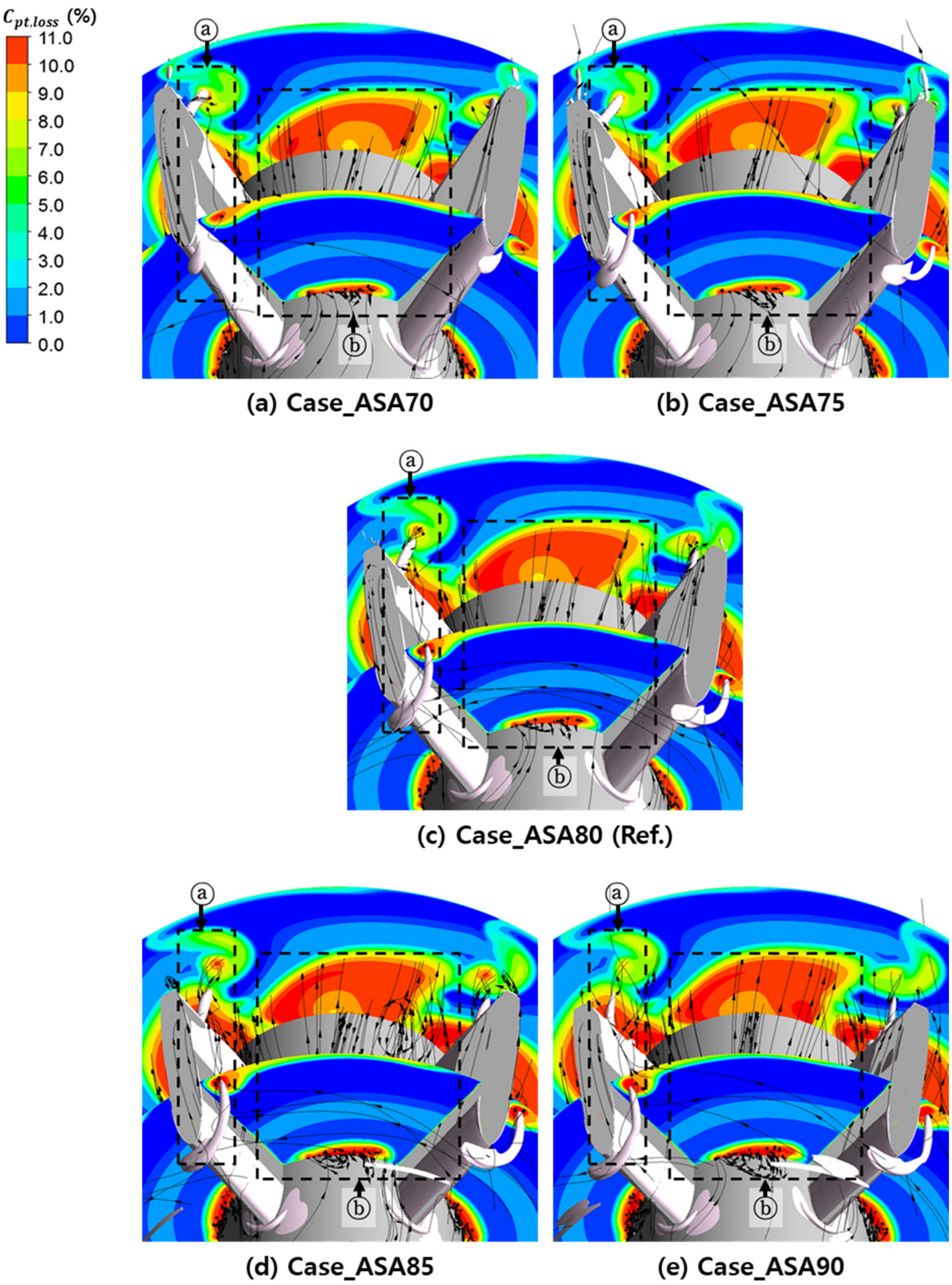

Figure 20. $C_{pt,loss}$ contours at x/L = 0.3 & 0.8 for the derived struts with varying swept angles.

4.4. Diffuser Hade Angle

Diffusion in the annular diffuser is able to occur due to increases in the cross-sectional area that occur according to the hade angle of the diffuser. The reference diffuser had two sections with different hade angles, as shown in Figure 2d. The first diffuser hade angle (θ_{h1}) of the reference diffuser was 19°, and this remained fixed throughout this study, the second (θ_{h1}) was 12°. The reference and derived diffusers are denoted by the prefix for the diffuser hade angle (DHA) followed by the value of their second hade angle. The shapes of each derived diffuser are shown in Figure 21, and the diffuser names and the shape information for all the derived diffusers are shown in Table 6. The other design parameters are the same as the reference diffuser.

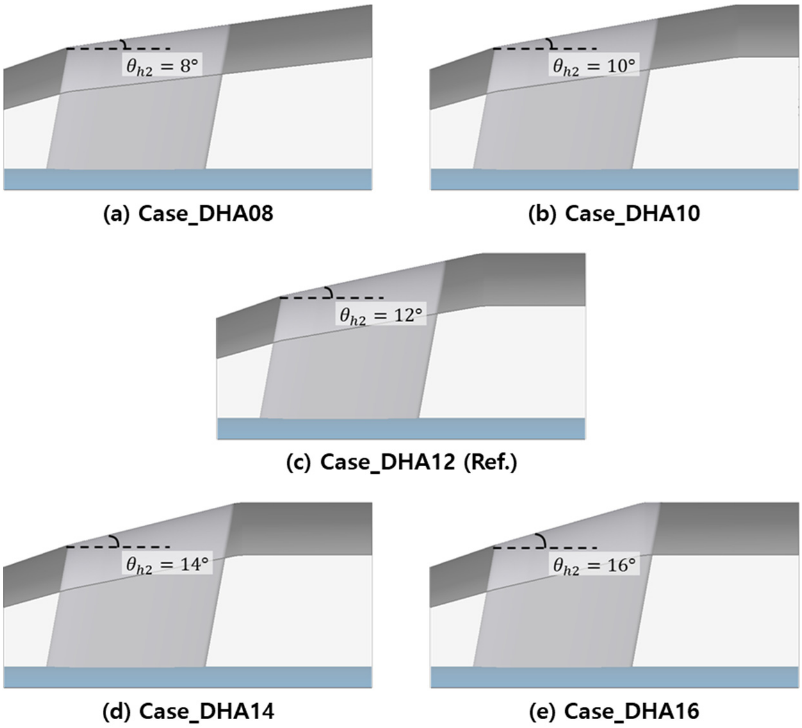

Figure 21. Schematics of the derived diffusers with varying hade angles.

Table 6. Geometry information of the reference and derived diffusers with varying hade angles.

Model	Case_DHA08	Case_DHA10	Case_DHA12 (Ref.)	Case_DHA14	Case_DHA16
Hade angle	8°	10°	12°	14°	16°

The mass-averaged C_p and $C_{pt,loss}$ plots over the normalized distance of the cross-sectional planes for the diffusers with varying hade angles are illustrated in Figures 22 and 23, respectively. The C_p and $C_{pt,loss}$ calculated at the conical diffuser outlet were expected to change as the diffuser hade angle changed, however, the results did not show much difference between the diffusers because of the flow characteristics at the diffuser inlet, as shown in Figure 5, combined with the existence of the struts. All models met the C_p design target of 0.75 or more, but the differences between the diffusers were small compared to the changes seen when the other design parameters were varied. The $C_{pt,loss}$ value for all of the derived diffusers was lower than the design target of 4%, but the gap between the models was small.

To evaluate the change in the flow field according to changes in the diffuser hade angle, the $C_{pt,loss}$ contours at a cross-sectional plane with a normalized distance of 1.0, 5.0, and 8.5 are shown in Figure 24. We can see a high $C_{pt,loss}$ region near the hub of the annular diffuser at the $x/L = 1.0$ plane and the center of the conical diffuser at the $x/L = 5.0$ plane. For the DHA08 model, the high $C_{pt,loss}$ region at the $x/L = 1.0$ plane is the smallest while the contour patterns of the other diffusers are mostly similar. This trend can also be seen at the $x/L = 5.0$ plane. The $C_{pt,loss}$ contour patterns, however, are similar for all diffusers as the pressure recovery due to diffusion proceeds. For the DHA10 model, there remains a high $C_{pt,loss}$ region at the $x/L = 8.5$ plane due to the extension of the high $C_{pt,loss}$ flow from the strut. Figure 25 shows the $C_{pt,loss}$ contours at Plane 1 with the velocity contours at the $x/L = 1.0$, 5.0, and 8.5 planes. As shown in the dashed line circle, there exists the high $C_{pt,loss}$ flow from the strut which has the low momentum. The flow influences the high $C_{pt,loss}$ flow in the hub region afterwards, and has the greatest influence in the DHA10 strut.

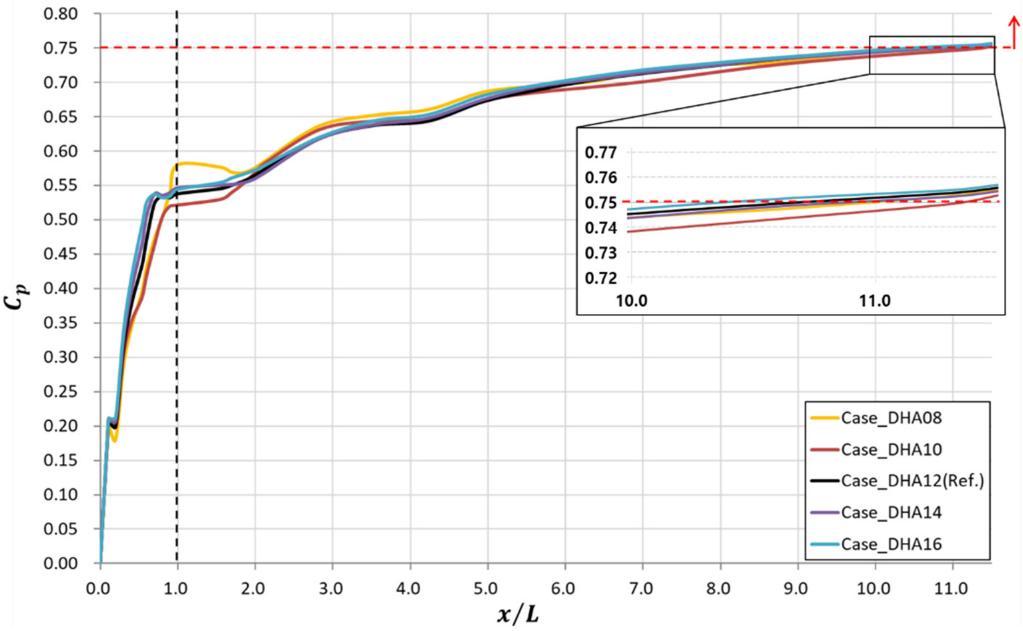

Figure 22. C_p plot for the derived diffusers with varying hade angles.

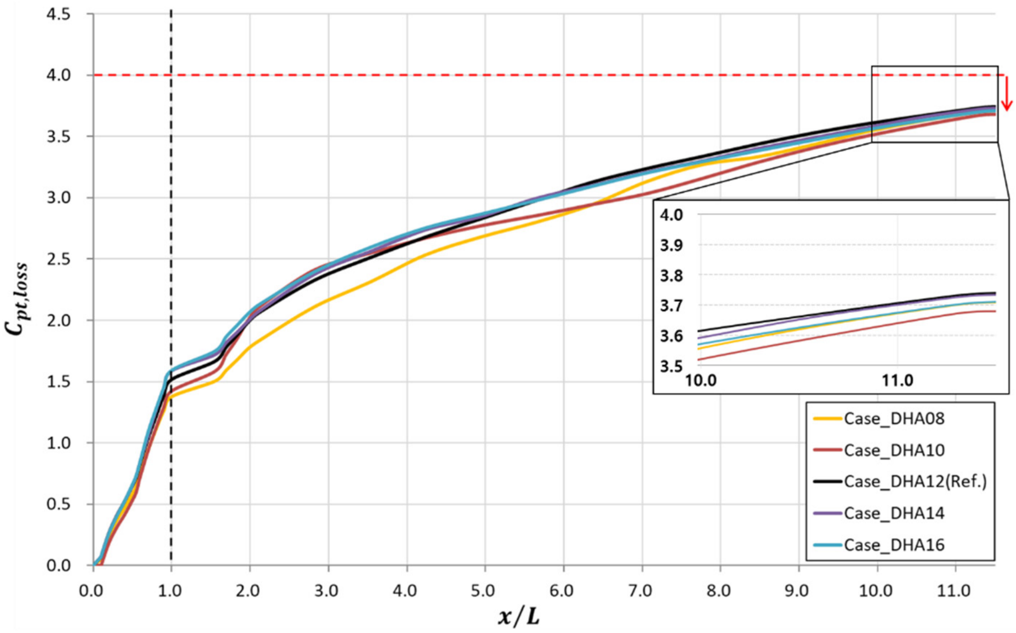

Figure 23. $C_{pt,loss}$ plot for the derived diffusers with varying hade angles.

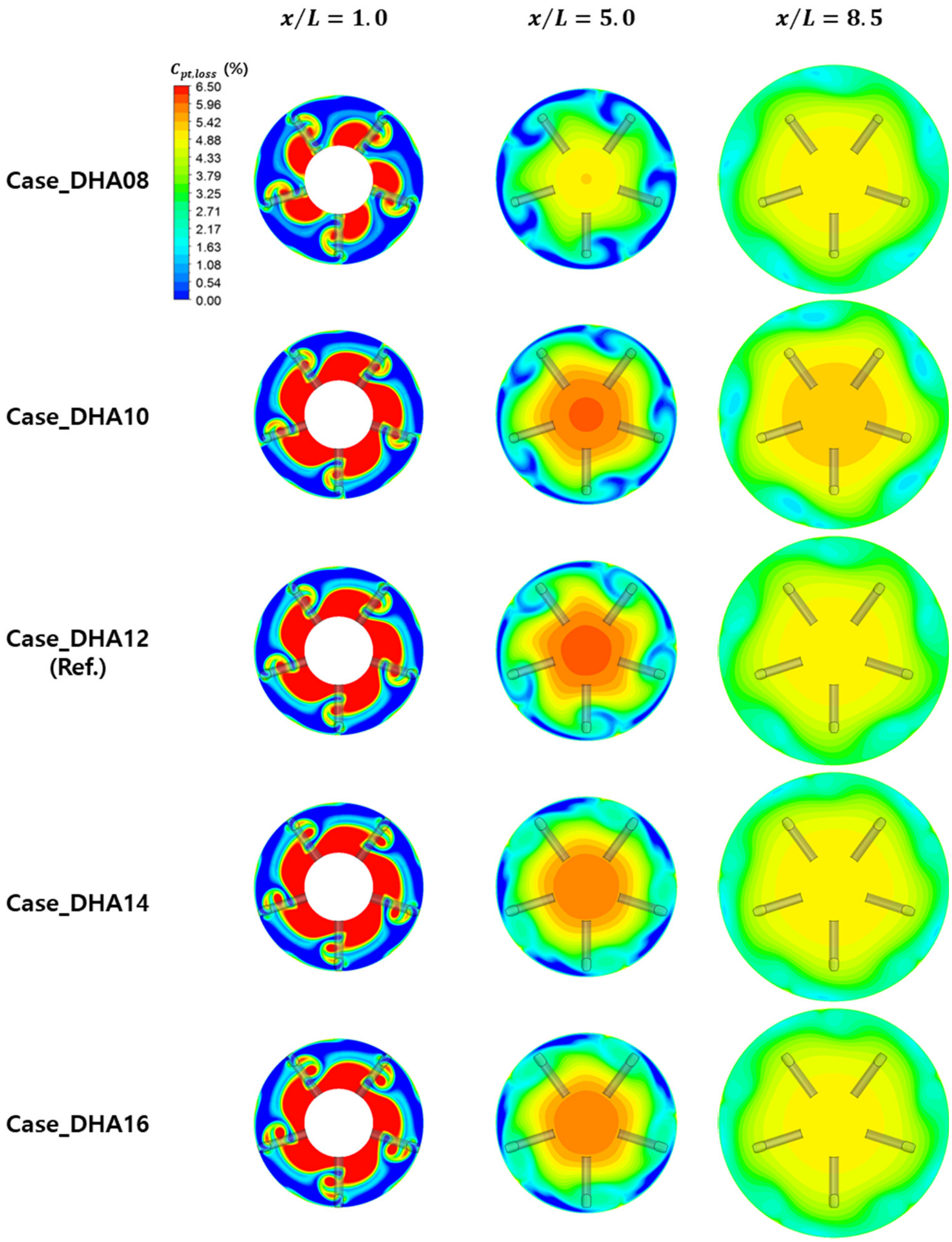

Figure 24. $C_{pt,loss}$ contours at $x/L = 1.0$, 5.0 and 8.5 for the derived diffusers with varying hade angles.

4.5. Evaluation of the Influence of Geometric Parameters

The effect of changes to the geometric parameters on pressure recovery and the total pressure loss of the turbine exhaust diffuser are plotted on the graphs in Figures 26 and 27, respectively. The mass-averaged C_p and $C_{pt,loss}$ calculated at the conical diffuser outlet for all derived models were normalized in relation to the reference model. Changes in the strut thickness and strut swept angle were found to have a large influence on C_p and $C_{pt,loss}$, whereas the diffuser hade angle only had only a very slight influence. Moreover, applying a strut lean angle affected both C_p and $C_{pt,loss}$ negatively. In summary, it is possible to enhance the aerodynamic performance of turbine exhaust diffusers by designing struts with the optimum thickness and swept angle.

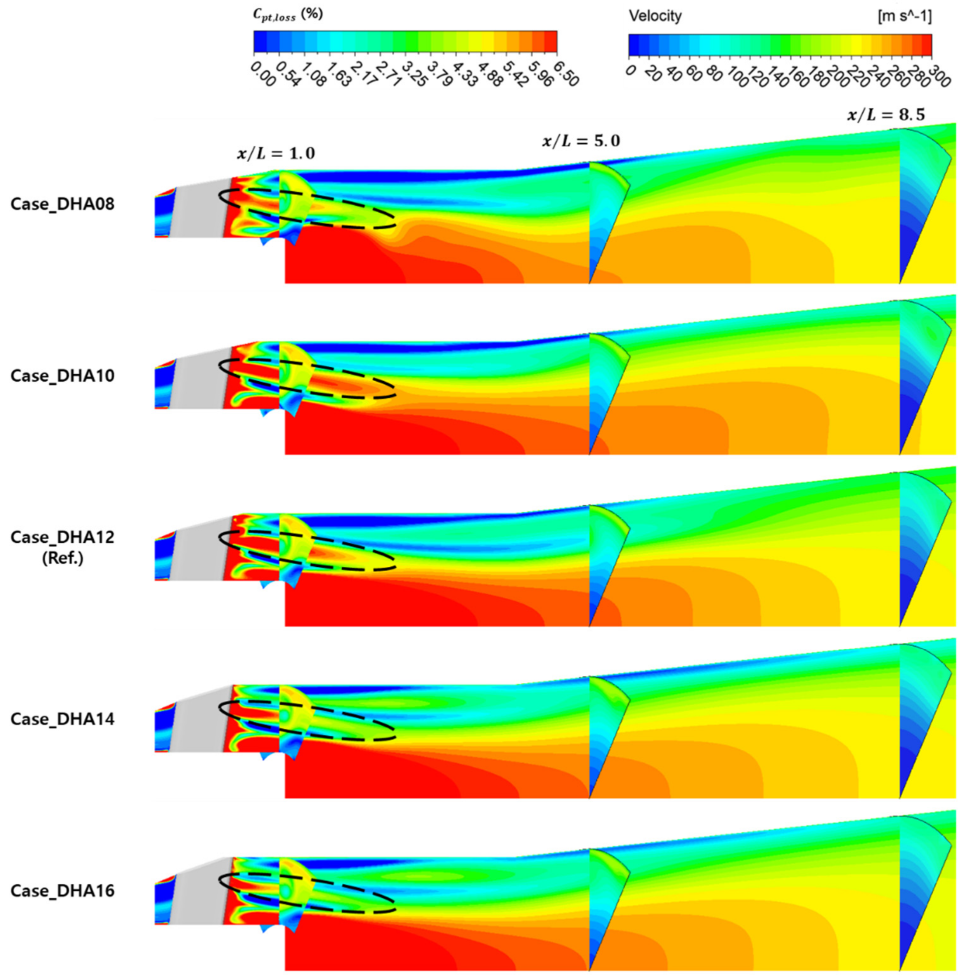

Figure 25. $C_{pt,loss}$ contours at Plane 1 with velocity contours at x/L = 1.0, 5.0 and 8.5 for the derived struts of varying diffuser hade angles.

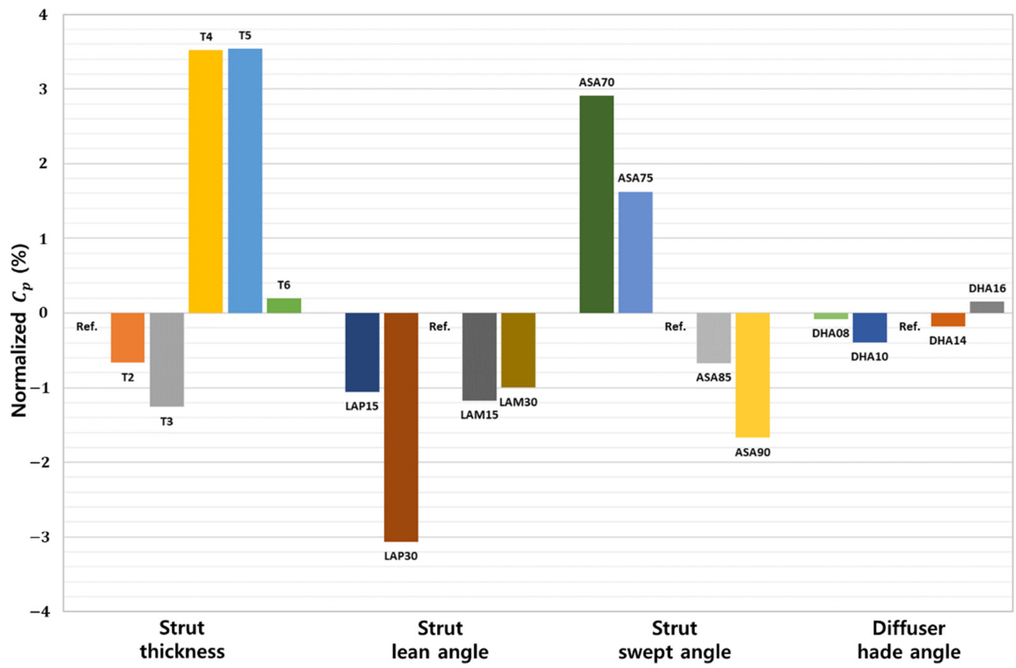

Figure 26. Comparison of normalized C_p with respect to the reference.

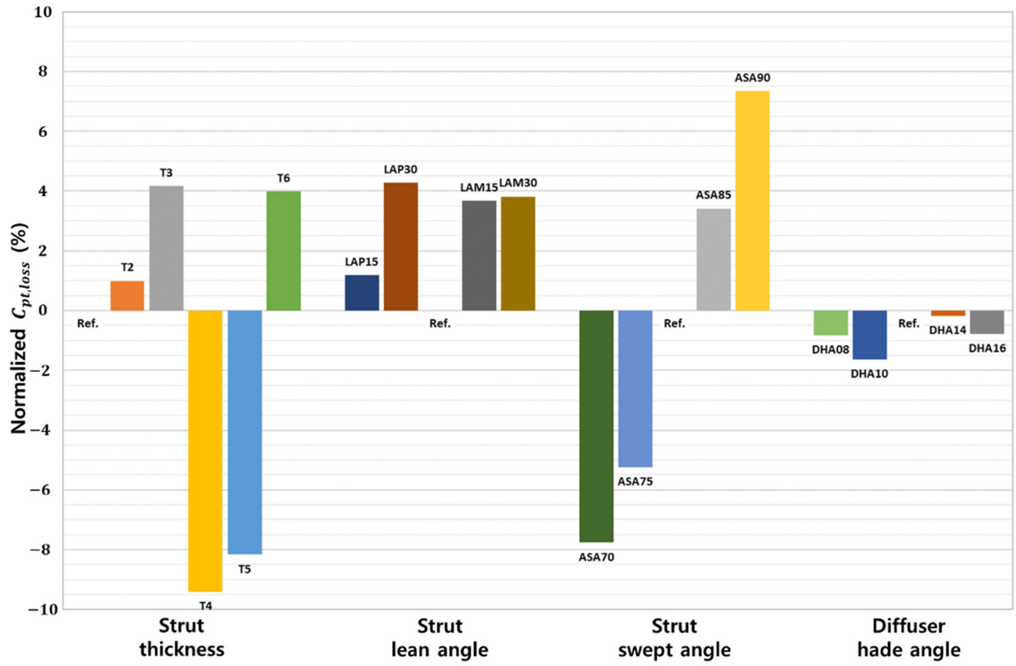

Figure 27. Comparison of normalized $C_{pt,loss}$ with respect to the reference.

5. Conclusions

Numerical simulations of turbine exhaust diffusers for H-class gas turbines were conducted to investigate the effect of geometric variations on their aerodynamic performance at the design point. The design targets for the turbine exhaust diffusers were a C_p of 0.75 or more and a $C_{pt,loss}$ of 4% or less. The strut thickness, strut lean angle, strut swept angle, and diffuser hade angle were selected as the parameters varied in this study.

- When varying strut thickness, there is a conflict between the performance enhancement gained by increasing the axial velocity between the struts and the performance degradation caused by the wake generated at the strut trailing edge. We expect that there is an optimal strut thickness that gives the maximum C_p and minimum $C_{pt,loss}$. In the present study, the Case_T4 strut, which was 1.4 times thicker than the reference strut, produced an increase of 3.5% in C_p and a decrease of 8.9% in $C_{pt,loss}$ compared to the reference.
- Applying a lean angle to the struts was shown to have a negative effect on aerodynamic performance in terms of both the pressure recovery and the total pressure loss.
- When the strut swept angle was increased, the total pressure loss due to horseshoe vortexes generated at the strut leading edge near the casing and the total pressure loss due to separation at the annular diffuser hub both increased. In the present study, the Case_ASA70 strut, which had a strut swept angle of 70° provided an increase of 2.9% in C_p and a decrease of 7.8% in $C_{pt,loss}$ compared to the reference.
- When the diffuser hade angle was varied, no definite effects on performance were found, and the C_p and $C_{pt,loss}$ at the conical diffuser remained much the same.

Based on the current study, it was found that the design parameters of the strut thickness and the strut swept angle for turbine exhaust diffusers play an important role in increasing C_p and decreasing $C_{pt,loss}$. Therefore, an optimization procedure is required using the current data to find the optimal strut geometry for improving the pressure recovery and reducing the pressure loss throughout the turbine exhaust diffuser.

Author Contributions: Conceptualization, methodology, software, writing—original draft preparation, B.J.L.; writing—review and editing, supervision, J.T.C. Both authors have read and agreed to the published version of the manuscript.

Funding: This research received no external funding.

Institutional Review Board Statement: Not applicable.

Informed Consent Statement: Not applicable.

Data Availability Statement: Not applicable.

Conflicts of Interest: The authors declare no conflict of interest.

References

1. Ubertini, S.; Desideri, U. Experimental performance analysis of an annular diffuser with and without struts. *Exp. Therm. Fluid Sci.* **2000**, *22*, 183–195. [CrossRef]
2. Vassiliev, V.; Irmisch, S.; Claridge, M.; Richardson, D.P. Experimental and Numerical Investigation of the Impact of Swirl on the Performance of Industrial Gas Turbines Exhaust Diffusers. In Proceedings of the ASME Turbo Expo 2003, Collocated with the 2003 International Joint Power Generation Conference, Atlanta, GA, USA, 16–19 June 2003; pp. 19–29.
3. Vassiliev, V.; Rothbrust, M.; Irmisch, S. Refitting of Exhaust Diffuser of Industrial Gas Turbine. In Proceedings of the ASME Turbo Expo 2008: Power for Land, Sea, and Air, Berlin, Germany, 9–13 June 2008; pp. 979–987.
4. Sieker, O.; Seume, J.R. Effects of Rotating Blade Wakes on Separation and Pressure Recovery in Turbine Exhaust Diffusers. In Proceedings of the ASME Turbo Expo 2008: Power for Land, Sea, and Air, Berlin, Germany, 9–13 June 2008; pp. 1921–1931.
5. Kluß, D.; Stoff, H.; Wiedermann, A. Effect of Wakes and Secondary Flow on Re-attachment of Turbine Exit Annular Diffuser Flow. *ASME J. Turbomach.* **2009**, *131*, 041012. [CrossRef]
6. Pradeep, A.M.; Roy, B.; Vaibhav, V.; Srinuvasu, D. Study of Gas Turbine Exhaust Diffuser Performance and Its Enhancement by Shape Modifications. In Proceedings of the ASME Turbo Expo 2010: Power for Land, Sea, and Air, Glasgow, UK, 14–18 June 2010; pp. 1101–1110.
7. Babu, M.; Shukla, R.K.; Maru, A.; Pradeep, A.M.; Roy, B. Boundary Layer Control in Turbine Exhaust Diffusers Using Casing Injection and Design Modifications. In Proceedings of the ASME Turbo Expo 2012: Turbine Technical Conference and Exposition, Copenhagen, Denmark, 11–15 June 2012; pp. 1069–1079.
8. Hirschmann, A.; Volkmer, S.; Casey, M.; Montgomery, M. Hub Extension in an Axial Gas Turbine Diffuser. In Proceedings of the ASME Turbo Expo 2012: Turbine Technical Conference and Exposition, Copenhagen, Denmark, 11–15 June 2012; pp. 1229–1238.
9. Schaefer, P.; Hofmann, W.H.; Gieß, P. Multiobjective Optimization for Duct and Strut Design of an Annular Exhaust Diffuser. In Proceedings of the ASME Turbo Expo 2012: Turbine Technical Conference and Exposition, Copenhagen, Denmark, 11–15 June 2012; pp. 1679–1689.
10. Vassiliev, V.; Irmisch, S.; Abdel-Wahab, S.; Granovskiy, A. Impact of the Inflow Conditions on the Heavy-Duty Gas Turbine Exhaust Diffuser Performance. *ASME J. Turbomach.* **2012**, *134*, 041018. [CrossRef]
11. Hirschmann, A.; Volkmer, S.; Schatz, M.; Finzel, C.; Casey, M.; Montgomery, M. The Influence of the Total Pressure Profile on the Performance of Axial Gas Turbine Diffusers. *ASME J. Turbomach.* **2012**, *134*, 021017. [CrossRef]
12. Dobhal, S.; Pradeep, A.M.; Roy, B. Effect of Geometry Changes in an Aggressive Turbine Exhaust Delivery System. In Proceedings of the ASME Turbo Expo 2013: Turbine Technical Conference and Exposition, San Antonio, TX, USA, 3–7 June 2013; p. V06AT36A005.
13. Xu, L.; Hedlund, L.; Nilsson, Å. CFD Investigation of the Influence of Inflow Conditions on an Aggressive Axial Exhaust Diffuser for Steam Turbines. In Proceedings of the ASME Turbo Expo 2014: Turbine Technical Conference and Exposition, Düsseldorf, Germany, 16–20 June 2014; p. V01BT27A038.
14. Schaefer, P.; Gieß, P.; Finzel, C.; Hofmann, W.H. Some Aspects on Inlet Blockage Affecting the Performance of a Heavy Duty Gas Turbine's Exhaust Diffuser. In Proceedings of the ASME Turbo Expo 2014: Turbine Technical Conference and Exposition, Düsseldorf, Germany, 16–20 June 2014. V02CT38A016.
15. Vassiliev, V.; Sommer, T.P.; Granovsky, A.; Prozorov, S. Exhaust Diffuser Characteristics at Off-Design Conditions. In Proceedings of the ASME Turbo Expo 2014: Turbine Technical Conference and Exposition, Düsseldorf, Germany, 16–20 June 2014; p. V02CT38A026.
16. Rasouli Ghazi Kalayeh, K.; Schäfer, P.; Finzel, C.; Hofmann, W.H. Experimental and numerical study of a gas turbine exhaust diffuser applying different hub extension geometries. In Proceedings of the 11th European Conference on Turbomachinery Fluid dynamics & Thermodynamics, Madrid, Spain, 23–27 March 2015.
17. Xue, S.; Guillot, S.; Ng, W.F.; Fleming, J.; Todd Lowe, K.; Samal, N.; Stang, U.E. An Experimental Investigation of the Performance Impact of Swirl on a Turbine Exhaust Diffuser/Collector for a Series of Diffuser Strut Geometries. *ASME J. Eng. Gas Turbines Power* **2016**, *138*, 092603. [CrossRef]
18. Siorek, M.P.; Guillot, S.; Xue, S.; Ng, W.F. A Sensitivity Study of Gas Turbine Exhaust Diffuser-Collector Performance at Various Inlet Swirl Angles and Strut Stagger Angles. *ASME J. Eng. Gas Turbines Power* **2018**, *140*, 072602. [CrossRef]
19. Mihailowitsch, M.; Schatz, M.; Vogt, D.M. Numerical Investigations of an Axial Exhaust Diffuser Coupling the Last Stage of a Generic Gas Turbine. *ASME J. Eng. Gas Turbines Power* **2019**, *141*, 031025. [CrossRef]

20. Bauer, M.; Hummel, S.; Schatz, M.; Kegalj, M.; Vogt, D.M. Investigation of the Flow Field and the Pressure Recovery in a Gas Turbine Exhaust Diffuser at Design, Part-Load and Over-Load Condition. In Proceedings of the ASME Turbo Expo 2020: Turbomachinery Technical Conference and Exposition. Volume 2D: Turbomachinery, Virtual, Online, 21–25 September 2020; p. V02DT36A009.
21. Sutherland, W. The viscosity of gases and molecular force. *Philos. Mag.* **1893**, *5*, 507–531. [CrossRef]
22. Xu, L.; Xiong, Y.; Xi, L.; Gao, J.; Li, Y.; Zhao, Z. Numerical Simulation of Swirling Impinging Jet Issuing from a Threaded Hole under Inclined Condition. *Entropy* **2020**, *22*, 15. [CrossRef] [PubMed]
23. Gamannossi, A.; Amerini, A.; Mazzei, L.; Bacci, T.; Poggiali, M.; Andreini, A. Uncertainty Quantification of Film Cooling Performance of an Industrial Gas Turbine Vane. *Entropy* **2020**, *22*, 16. [CrossRef] [PubMed]
24. Zamiri, A.; Park, K.S.; Choi, M.; Chung, J.T. Transient Analysis of Flow Unsteadiness and Noise Characteristics in a Centrifugal Compressor with a Novel Vaned Diffuser. *Appl. Sci.* **2021**, *11*, 3191. [CrossRef]
25. Norheim, S.; Amzin, S. Numerical Investigation of a Radially Cooled Turbine Guide Vane Using Air and Steam as a Cooling Medium. *Computation* **2021**, *9*, 63. [CrossRef]
26. Wei, Z.; Ren, G.; Gan, X.; Ni, M.; Chen, W. Influence of Shock Wave on Loss and Breakdown of Tip-Leakage Vortex in Turbine Rotor with Varying Backpressure. *Appl. Sci.* **2021**, *11*, 4991. [CrossRef]